ELSEVIER

Soil Dynamics and Earthquake Engineering 28 (2008) 20–35

SOIL DYNAMICS AND EARTHQUAKE ENGINEERING

www.elsevier.com/locate/soildyn

Parameterization of the porous-material model for sand with different levels of water saturation

M. Grujicic[a,*], B. Pandurangan[a], R. Qiao[a], B.A. Cheeseman[b], W.N. Roy[b], R.R. Skaggs[b], R. Gupta[b]

[a]*Department of Mechanical Engineering, Clemson University, Clemson, SC 29634, USA*
[b]*Army Research Laboratory—Survivability Materials Branch, Aberdeen, Proving Ground, MD 21005-5069, USA*

Received 2 January 2007; received in revised form 26 April 2007; accepted 7 May 2007

Abstract

The experimental results for the mechanical response of sand (at different levels of saturation with water) under shock-loading conditions generated by researchers at Cavendish [Bragov AM, Lomunov AK, Sergeichev IV, Tsembelis K, Proud WG. The determination of physicomechanical properties of soft soils from medium to high strain rates, November 2005, in preparation; Chapman DJ, Tsembelis K, Proud WG. The behavior of water saturated sand under shock-loading. In: Proceedings of the 2006 SEM annual conference and exposition on experimental and applied mechanics, vol. 2, 2006.p.834–40] are used to parameterize our recently developed material model for sand [Grujicic M, Pandurangan B, Cheeseman B. The effect of degree of saturation of sand on detonation phenomena associated with shallow-buried and ground-laid mines. J Shock Vib 2006;13:41–61]. The model was incorporated into a general-purpose non-linear dynamics simulation program to carry out a number of simulation analyses pertaining to the detonation of a landmine buried in sand and to the interactions of the detonation products, mine fragments and sand ejecta with various targets. A comparison of the computed results with their experimental counterparts revealed a somewhat improved agreement with the experimental results in the case of the present model as compared to the agreement between the widely used porous-material/compaction model for sand and the experiments.

Keywords: Sand; Material model; Detonation; Shallow-buried mine; Blast loading

1. Introduction

Recent advances in numerical analysis capabilities, particularly the coupling of Eulerian solvers (used to model gaseous detonation products and air) and Lagrangian solvers (used to represent vehicles/platforms and soil), have allowed simulations to provide insight into complex loading created by the mine blast event. However, a quantified understanding of the blast phenomena and loadings through computer modeling is still not mature. As discussed in our previous work [3], the lack of maturity of computer simulations of the blast event is mainly due to inability of the currently available materials models to realistically represent the response of the materials involved under high deformation, high-deformation rate, high-temperature conditions, and the type of conditions accompanying landmine detonation.

The knowledge of the mechanical response of sand (or soil in general) under shock/blast loading conditions is critical in many engineering disciplines and commercial and military endeavors (e.g. mining, construction, design of survivable armored vehicles, etc.). For many years, the common practice was to develop purely empirical relations for soil at a given site using a variety of (non-standardized) experimental tests. Such relations are often found to have very little portability and may, when used in soil and test conditions different from the original ones, lead to widely different and unrealistic predictions [4,5]. To overcome these severe limitations, over the last dozen years general researchers have attempted to develop a constitutive material model for sand, which could include various

*Corresponding author. Tel.: +1 864 656 5639; fax: +1 864 656 4435.
E-mail address: mica.grujicic@ces.clemson.edu (M. Grujicic).

0267-7261/$ - see front matter © 2007 Elsevier Ltd. All rights reserved.
doi:10.1016/j.soildyn.2007.05.001

Report Documentation Page

Form Approved
OMB No. 0704-0188

1. REPORT DATE	2. REPORT TYPE	3. DATES COVERED
2008		**00-00-2008 to 00-00-2008**

4. TITLE AND SUBTITLE	5a. CONTRACT NUMBER
Parameterization of the porous-material model for sand with different levels of water saturation	5b. GRANT NUMBER
	5c. PROGRAM ELEMENT NUMBER
6. AUTHOR(S)	5d. PROJECT NUMBER
	5e. TASK NUMBER
	5f. WORK UNIT NUMBER
7. PERFORMING ORGANIZATION NAME(S) AND ADDRESS(ES) **Celmson University,Department of Mechanical Engineering,Clemson,SC,29634**	8. PERFORMING ORGANIZATION REPORT NUMBER
9. SPONSORING/MONITORING AGENCY NAME(S) AND ADDRESS(ES)	10. SPONSOR/MONITOR'S ACRONYM(S)
	11. SPONSOR/MONITOR'S REPORT NUMBER(S)

12. DISTRIBUTION/AVAILABILITY STATEMENT
Approved for public release; distribution unlimited

13. SUPPLEMENTARY NOTES

14. ABSTRACT

The experimental results for the mechanical response of sand (at different levels of saturation with water) under shock-loading conditions generated by researchers at Cavendish [Bragov AM, Lomunov AK, Sergeichev IV, Tsembelis K, Proud WG. The determination of physicomechanical properties of soft soils from medium to high strain rates, November 2005, in preparation; Chapman DJ, Tsembelis K, Proud WG. The behavior of water saturated sand under shock-loading. In: Proceedings of the 2006 SEM annual conference and exposition on experimental and applied mechanics, vol. 2, 2006.p.834?40] are used to parameterize our recently developed material model for sand [Grujicic M, Pandurangan B, Cheeseman B. The effect of degree of saturation of sand on detonation phenomena associated with shallow-buried and ground-laid mines. J Shock Vib 2006;13:41?61]. The model was incorporated into a general-purpose non-linear dynamics simulation program to carry out a number of simulation analyses pertaining to the detonation of a landmine buried in sand and to the interactions of the detonation products, mine fragments and sand ejecta with various targets. A comparison of the computed results with their experimental counterparts revealed a somewhat improved agreement with the experimental results in the case of the present model as compared to the agreement between the widely used porous-material/compaction model for sand and the experiments.

15. SUBJECT TERMS

16. SECURITY CLASSIFICATION OF:			17. LIMITATION OF ABSTRACT	18. NUMBER OF PAGES	19a. NAME OF RESPONSIBLE PERSON
a. REPORT **unclassified**	b. ABSTRACT **unclassified**	c. THIS PAGE **unclassified**	**Same as Report (SAR)**	**16**	

Nomenclature

α	porosity
β	saturation ratio
C	speed of sound
e	internal energy
η	compression ratio
Γ	Gruneisen gamma
P	pressure
φ	yield stress to pressure proportionality coefficient
ρ	density
s	slope of $U_s - U_p$ relationship
σ	yield stress
V	volume
x	spatial coordinate
y	spatial coordinate

Subscripts

Bulk	bulk material quantity
Comp	value at full compaction
dry	dry sand quantity
fail	failure-related quantity
H	Hugoniot quantity
MC	Mohr–Coulomb value
0	initial value
p	pore-related quantity
ref	fully compacted sand-related quantity
sat	saturation related quantity
Unsat	unsaturated sand-related quantity
w	water-related quantity

aspects of sand composition/microstructure and the moisture and organic matter contents (e.g. [1–5]).

Sand has generally a complex structure consisting of mineral solid particles, which form a skeleton. The pores between the solid particles are filled with a low-moisture air (this type of sand is generally referred to as "dry sand"), with water containing a small fraction of air ("saturated sand") or comparable amounts of water and air ("unsaturated sand"). The relative volume fractions of the three constituent materials in the sand (the solid mineral particles, water and air) are generally quantified by the porosity, α, and the degree of saturation (saturation ratio), β, which are, respectively, defined as

$$\alpha = \frac{V_p}{V} \tag{1}$$

and

$$\beta = \frac{V_w}{V_p}, \tag{2}$$

where V_p is the volume of void (pores), V_w is the volume of water and V is the total volume.

Surface roughness and the presence of inorganic/organic binders are generally considered to be the main causes for friction/adhesion at the inter-particle contacting surfaces. Deformation of the sand is generally believed to involve two main basic mechanisms [4,5]: (a) elastic deformations (at low-pressure levels) and fracture (at high-pressure levels) of the inter-particle bonds and (b) elastic and plastic deformations of the three constituent materials in the sand. The relative contributions of these two deformation mechanisms as well as their behavior are affected primarily by the degree of saturation of sand and the deformation rate. Specifically, in dry sand, the first mechanism controls the sand deformation at low pressures while the second mechanism is dominant at high pressures and the effect of deformation rate is of a second order. In sharp contrast, in saturated sand, very low inter-particle friction diminishes the role of the first deformation mechanism. On the other hand, the rate of deformation plays an important role. At low deformation rates (of the order of $1.0 \times 10^{-3}\,s^{-1}$), the water/air residing in the sand pores is squeezed out during deformation and, consequently, the deformation of the sand is controlled by the deformation of the solid mineral particles. At high deformation rates (of the order of $1.0 \times 10^{5}\,s^{-1}$) and pressures (of the order of ca. 1 GPa), on the other hand, water/air is trapped within the sand pores and the deformation of the sand is controlled by the deformation and the volume fractions of each of the three constituent phases.

In the areas of soil mechanics and soil dynamics, it is often assumed that the solid particles do not undergo plastic deformation and that the water phase is incompressible. The external loading is internally supported by the soil skeleton (via the so-called "effective stress" and by the water (via the so-called "pore pressure") [6]. Furthermore, the deformation of soil is controlled by the effective stress since the water and gas do not support any shear loading and are capable of flowing out through the soil pores. A number of investigators (e.g. [4,5]) clearly established that the effective stress approach discussed above is correct under the static/quasi-static loading conditions but it becomes deficient under shock-loading conditions. The two key deficiencies of the effective stress approach are the inability to account for: (a) deformation of the solid particles under shock loads and (b) the fact that due to a very short duration of shock loading, water may become trapped in soil pores and provide additional load support.

To overcome these limitations of the effective stress approach, Wang et al. [4,5], proposed a so-called "three-phase soil model". The model includes an *Equation of State* (based on the conceptual approach developed by Henrych [7]), a Drucker–Prager type strength model [8] and a damage model for degradation of strength and stiffness of the soil skeleton. Despite its solid physical foundation, the three-phase model was not widely accepted in the

military-engineering communities, primarily due to its excessive mathematical complexity and uncertainty regarding the reliability of the values for the key model parameters.

The most widely used soil material model in the military communities is the so-called "porous-material/compaction" model developed by Laine and Sandvik [9]. The model was constructed using the experimental results (from a variety of high-rate loading tests) to both ascertain the nature of the underlying functional relationships and to determine (via a multi-regression analysis) the magnitude of the model parameters.

As mentioned above, the porous-material/compaction model for sand proposed by Laine and Sandvik [9] has been, for quite some time, the sand model, which provided the best compromise between the inclusion of essential physical phenomena reflecting material response under dynamic loading and computational simplicity. However, the model of Laine and Sandvik [9] was developed essentially for dry sand and, as determined by many researchers (e.g. [10–12]), it cannot account for the effect of moisture content. To overcome this deficiency of the original porous-material/compaction model, Clemson University and the Army Research Laboratory, Aberdeen, Proving Ground, MD [3] jointly developed a modified version of Laine and Sandvik model to account for the effect of degree of sand saturation. The original parameterization of this model (referred to as the CU-ARL sand model hereafter) was done using a variety of experimental data as well as first principles type estimations. Recently, a detailed investigation of dynamic response of sand at different saturation levels was carried out by researchers at the Cavendish Laboratory, Cambridge, UK [1,2]. The experimental data obtained provide an excellent opportunity to reassess the parameters in the CU-ARL sand model. Such parameter reassessment is the subject of the present work.

The organization of the paper is as follows. The procedure and the results of the CU-ARL sand model parameterization analysis are presented and discussed in Section 2. Incorporation of the CU-ARL sand model into a transient non-linear dynamics computer program and its use in the simulation of a number of buried-land mine blast scenarios along with experimental results are all presented in Section 3. A brief summary and the conclusions obtained in the present work are discussed in Section 5.

2. CU-ARL model parameterization

The complete formulation of a transient non-linear dynamics problem such as the interaction between detonation products, landmine fragments and soil ejecta with a target structure entails the knowledge of materials models (material-specific relations between pressure, deviatoric stress, mass density, strain, strain rate, internal energy density, etc.). These relations typically involve: (a) an equation of state, (b) a strength equation, (c) a failure equation and (d) an erosion equation for each constituent material. The equation of state defines pressures dependence on mass density and internal-energy density (and in the case of anisotropic materials, on deviatoric strain). The strength and failure equations define the evolutions of the deviatoric stress in the elastic regime, elastic–plastic regime, and in the post-failure initiation regime. In other words, the equation of state along with the strength and failure equations (as well as with the equations governing the onset of plastic deformation and failure and the plasticity and failure-induced material flow) enable assessment of the evolution of the complete stress tensor during a transient non-linear dynamics analysis. Such an assessment is needed where the governing conservation equations are being solved. The erosion equation is generally intended for eliminating numerical solution difficulties arising from highly disordered Lagrangian cells. Nevertheless, the erosion equation is often used to provide additional material failure mechanism especially in materials with limited ductility.

In this section, an effort is made to parameterize the CU-ARL sand model using the recently-made available experimental results [1,2]. To facilitate the implementation of the CU-ARL model into commercial and public-domain transient non-linear dynamics codes, the governing model relations are expressed in terms of the soil/state parameters: mass density at full compaction (referred to as the reference density), ρ_{ref}; (which accounts for the effect of the chemical composition of sand) the initial soil porosity, α_0, which is primarily controlled by the particles average size and distribution as well as the extent of soil pre-compaction and initial extent of soil water-saturation, β_0, as well as in terms of the model-defining parameters. It should be noted that the CU-ARL model is designated to account for the behavior of sand under high deformation-rate conditions under which the water is trapped in the inter-particles spaces.

2.1. Porous-material/compaction equation of state

Porous-material equation of state is a particular form of the Mie–Gruneisen equation of state

$$P = P_{\text{H}} + \Gamma\rho(e - e_{\text{H}}), \tag{3}$$

in which the second term on the right-hand side of Eq. (3) is omitted. In Eq. (3), the following nomenclature is used: P is the pressure (a sum of the pore pressure and effective stress in the soil skeleton), ρ is the (current) mass density, Γ is the Gruneisen gamma parameter, e is the internal energy density and the subscript H is used to denote the reference shock-Hugoniot level of a given quantity.

The Hugoniot pressure is defined using the following stationary-shock relationship [13]:

$$P_{\text{H}} = \frac{\rho_0 C_0^2 \eta}{(1 - s\eta)^2}, \tag{4}$$

where $\rho_0 = (1 - \alpha_0)\rho_{\text{ref}} + \alpha_0\beta_0\rho_{\text{w}}$ is the initial material mass density, where C_0 is the speed of sound (in the

homogenized sand/pores medium as measured using the standard flyer-plate experiment setup at room temperature [2]),

$$\eta = \left(1 - \frac{\rho_0 - \alpha_0\beta_0\rho_w}{\rho - \alpha_0\beta_0\rho_w}\right) = \left(1 - \frac{(1-\alpha_0)\rho_{ref}}{\rho - \alpha_0\beta_0\rho_w}\right)$$

is the compressibility ratio, ρ_w is the density of water and the parameter s represents a rate of increase of the (average) particles velocity, U_p, with an increase in the shock velocity, U_s, and is defined by the relation

$$U_s = C_0 + sU_p. \tag{5}$$

In the CU-ARL sand-model equation of state, the aforementioned relations for ρ_0 and η are substituted in Eq. (4) to get

$$P = P_H = \frac{((1-\alpha_0)\rho_{ref} + \alpha_0\beta_0\rho_w)C_0^2\left(1 - \frac{(1-\alpha_0)\rho_{ref}}{\rho - \alpha_0\beta_0\rho_w}\right)}{\left(1 - s\left(1 - \frac{(1-\alpha_0)\rho_{ref}}{\rho - \alpha_0\beta_0\rho_w}\right)\right)^2}, \quad \rho \leqslant \rho_{comp} \tag{6a}$$

and

$$P = P_H = P(\rho_{comp}) + C_0^2(\rho - \rho_{comp}), \quad \rho > \rho_{comp}, \tag{6b}$$

where

$$\rho_{comp} = \left(\frac{1-\alpha_0}{1-\alpha_0+\alpha_0\beta_0}\right)\rho_{ref} + \left(\frac{\alpha_0\beta_0}{1-\alpha_0+\alpha_0\beta_0}\right)\rho_w$$

is the density of the sand at full compaction. Full compaction is defined as a porosity-free state of sand.

The degree of saturation-dependent parameters C_0 and s are obtained by fitting the original U_s vs. U_p results obtained in Refs. [1,2] to a low-order polynomial in which the coefficients are set to depend on the initial level of porosity and the reference density. The results of this curve fitting procedure are given in Fig. 1(a) and (b), where the C_0 vs. β_0 and the s vs. β_0 functional relations are also given. These relations in conjunction with Eqs. (6a) and (6b) define the dependence of pressure on ρ_{ref}, α_0, β_0 and ρ.

The P vs. ρ relation just derived is valid only during loading and only when such loading gives rise to irreversible/plastic compaction of the porous material. It should be noted that the term loading implies an event within which the pressure is increased (and, in the case of plastic loading, a decrease in material porosity takes place). Conversely, unloading is associated with a decrease in pressure. As shown in our previous work [3], during unloading/elastic reloading, the P vs. ρ relationship is defined as $dp/d\rho = C_0^2(\rho_{ref},\alpha_0,\beta_0)$, where the $C_0(\rho_{ref},\alpha_0,\beta_0)$ relation is given in Fig. 1(a).

2.2. Porous-material/compaction strength model

Within the original compaction strength model for dry sand, the pressure dependence of yield stress is defined as [9]

$$\sigma_{y,dry} = \phi_{dry}P_{dry} \approx \begin{cases} 1.3732P_{dry}, & 0 < P_{dry} \leqslant P_{MC}, \\ 1.3732P_{MC}, & P_{dry} > P_{MC}. \end{cases} \tag{7}$$

Also for the saturated sand, as discussed in our previous work [12], the pressure-dependent yield stress can be defined as

$$\sigma_{y,sat} = \begin{cases} \phi_{sat}P_{sat}, & 0 \leqslant P_{sat} \leqslant P_{MC}, \\ \phi_{sat}P_{MC}, & P_{sat} > P_{MC}, \end{cases} \tag{8}$$

where the yield-stress-to-pressure proportionality coefficient, ϕ_{sat}, is defined as

$$\phi_{sat} = \begin{cases} \left(0.1 + 1.2732\frac{P_{sat}}{P_{MC}}\right), & 0 \leqslant P_{sat} \leqslant P_{MC}, \\ 1.3732, & P_{sat} > P_{MC}. \end{cases} \tag{9}$$

The term P_{MC} ($= 1.864 \times 10^5$ kPa) appearing in Eqs. (7)–(9) is the Mohr–Coulomb pressure beyond which the yield stress is pressure insensitive. It should be noted that neither of Eqs. (7)–(9) include the effect of strain rate on the yield strength of sand. This was justified in our previous work [3], where it was shown that as long as the model is used at high deformation rates (ca. $1.0 \times 10^3\,s^{-1}$), the strength and failure behavior of sand can be considered rate independent.

The yield stress vs. pressure relationship for the unsaturated sand can then be defined using a linear combination of the yield-stress/pressure proportionality coefficients in dry and the saturated sands as

$$\sigma_{y,unsat} = \begin{cases} \phi_{unsat}P_{unsat}, & 0 \leqslant P_{unsat} \leqslant P_{MC}, \\ \phi_{unsat}P_{MC}, & P_{unsat} > P_{MC}, \end{cases} \tag{10}$$

where

$$\phi_{unsat} = (1-\beta_0)\phi_{dry} + \beta_0\phi_{sat}. \tag{11}$$

Defined in this way, Eqs. (10) and (11) can be also used for dry sand ($\beta_0 = 0.0$) and saturated sand ($\beta_0 = 1.0$).

In addition to specifying the yield stress vs. pressure relationship, the compaction strength model entails the knowledge of the density-dependent shear modulus. Since water has no ability to support shear stresses, the shear modulus, G, of unsaturated sand is dominated by the shear modulus of the solid skeleton of the sand. However, the presence of water changes the density of the sand. Therefore, the original compaction shear modulus vs. density relationship (defined using 10 pairs of (G, ρ) points in AUTODYN) was fitted to a polynomial function and modified by: (a) correcting density with a $-\alpha_0\beta_0\rho_w$ term and (b) introducing a moisture-level dependent maximum shear modulus in order to obtain a (deformation-rate independent) shear modulus vs. density relationship for sand at different saturation levels. This procedure yielded

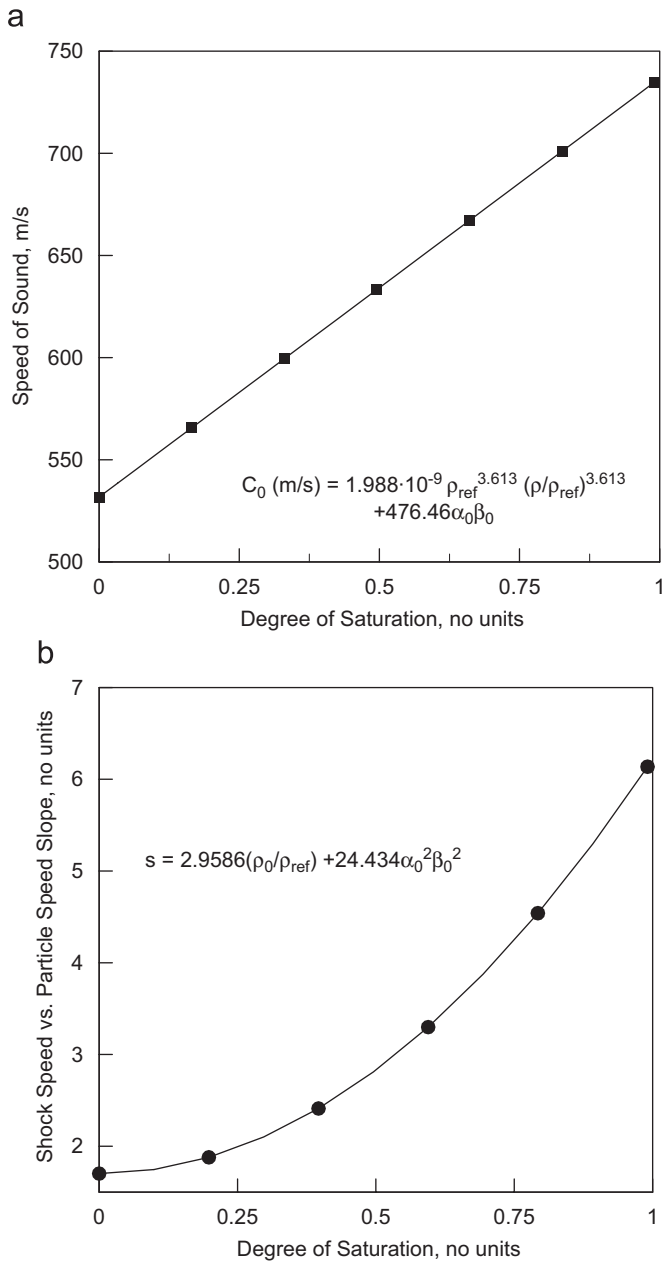

Fig. 1. Variation of the: (a) speed of sound and (b) the shock speed U_s vs. particles speed U_p slope with the initial degree of saturation of sand.

the following functional relationships:

$$G\,(\mathrm{kPa}) = \begin{cases} 5.2175\times10^{-14}(\rho-\alpha_0\beta_0\rho_w)^6, \\ \quad \rho(\mathrm{kg/m^3}) < (1-\alpha_0\beta_0)\rho_{ref}+\alpha_0\beta_0\rho_w, \\ (1-\alpha_0\beta_0)G_{Bulk}, \\ \quad \rho(\mathrm{kg/m^3}) \geqslant (1-\alpha_0\beta_0)\rho_{ref}+\alpha_0\beta_0\rho_w, \end{cases} \tag{12}$$

where G_{Bulk} ($=3.73470\times10^7$) denotes the shear modulus of fully compacted dry sand. Eq. (12) correctly accounts for the fact that, at full compaction, the sand density is equal to $(1-\alpha_0\beta_0)\rho_{ref}+\alpha_0\beta_0\rho_w$.

It should be noted that in the strength model developed in this section, the contribution of water to the material strength was neglected. This can be justified by recognizing the fact that viscosity of water is typically is around $0.001\,\mathrm{Pa\cdot s}$ and at deformation rates of $1.0\times10^5\,\mathrm{s^{-1}}$, the contribution of water to the shear strength of the sand is a mere 100 Pa.

2.3. Porous-material/compaction failure model

It is well established that the presence of moisture in sand increases the sand's cohesive strength [14]. Therefore, the magnitude of the (negative) failure pressure for sand is expected to increase with the saturation ratio (β). Also, the moisture content should be substantial ($\beta>0.7$) before its effect on the cohesive strength of sand becomes significant [14]. To account for these two observations, in our recent work [12], the following expression was proposed for the magnitude of the (negative) failure pressure in unsaturated sand, $P_{fail,\,unsat}$:

$$P_{fail,unsat} = \beta_0^5 P_{fail,sat}, \tag{13}$$

where $P_{fail,\,sat}$ (set equal to 729 kPa) is the failure pressure in saturated sand [14]. The relationship given by Eq. (13) correctly predicts that the cohesive strength of unsaturated sand with a saturation ratio of 0.7 is around 10–15% of that in the saturated sand.

2.4. Porous-material/compaction erosion model

Erosion of a porous-material element is assumed to take place when geometrical (i.e. elastic plus plastic plus damage) instantaneous strain reaches a maximum allowable value. Our prior investigation [10] established that the optimal value for the geometrical instantaneous strain is ~1.0. When a material element is eroded, its nodes are retained along with their masses and velocities in order to conserve momentum of the system. The momentum is conserved by distributing the mass and velocities associated with the eroded cells among the corner nodes of the remaining cells. Despite the fact that some loss of accuracy is encountered in this procedure (due to removal of the strain energy from the eroded elements), the procedure is generally found to yield reasonably accurate results [13].

3. CU-ARL model testing and validation

In this section, the CU-ARL sand model is tested by carrying out a number of computational simulations and by comparing the computed results with their experimental counterparts. All the calculations carried out in this section were done using AUTODYN, a general purpose non-linear dynamics modeling and simulation software [13]. In this section, a brief overview is given of the basic features of AUTODYN, emphasizing the aspects of this computer program, which pertain to the problem at hand.

A transient non-linear dynamics problem is analyzed within AUTODYN by solving simultaneously the governing partial differential equations for the conservation of momentum, mass and energy along with the materials

constitutive equations and the equations defining the initial and the boundary conditions. The equations mentioned above are solved numerically using a second-order accurate explicit scheme and one of the two basic mathematical approaches, the Lagrange approach and the Euler approach. Within AUTODYN these approaches are referred to as "processors". The key difference between the two basic processors is that within the Lagrange processor the numerical grid is attached to and moves along with the material during calculation while within the Euler processor, the numerical grid is fixed in space and the material moves through it. In our recent work [12], a brief discussion was given of how the governing differential equations and the materials constitutive models define a self-consistent system of equations for the dependent variables (nodal displacements, nodal velocities, cell material densities and cell internal energy densities).

In the present work, both the Lagrange and Euler processors are used. The Lagrange processor was used to model the sand and various targets and structural components. High-energy explosives, gaseous mine-detonation products and the surrounding air are modeled using the multi-material Euler processor. Different regions of the mine/air/target/sand model are allowed to interact and self-interact using the AUTODYN interaction options. A brief overview of the parts interactions and self-interactions AUTODYN algorithms can be found in our recent work [12]. Also a detailed description of the Lagrange and multi-material Euler processors as well as of the material models used for air, high explosives and metallic structural materials can be found in our recent work [11,12].

Throughout this manuscript, the terms "Depth of Burial" (DOB) and the "Stand-off Distance" (SOD) are used to denote distances between the mine top face and the sand/air interface, and between the sand/air interface and the bottom face of the target structure, respectively.

3.1. Total momentum transferred to the target structure

To assess the ability of the CU-ARL sand model to account for the total momentum transferred to the target structure following detonation of a ground-laid or shallow-buried mine at different saturation levels of the sand, the computational results are compared with their experimental counterparts obtained in Refs. [15,16].

3.1.1. Dry and unsaturated sand

To assess the ability of the CU-ARL sand model to account for the total momentum transferred to the target structure at low to medium saturation levels of the sand, a non-linear dynamics-based computational analysis of the interaction of detonation products, mine fragments and sand ejecta with an instrumented horizontal mine-impulse pendulum used in Ref. [15], is carried out and the computed results are compared with their experimental counterparts. Since a detailed description of the experimental details related to the construction and utilization of instrumented horizontal mine-impulse pendulum can be found in our recent work [12], they will not be presented here.

Next, a brief description is given of the computational model used to simulate the interaction of the detonation-products/soil ejecta resulting from the explosion of a shallow-buried or ground-laid mine and the instrumented horizontal mine-impulse pendulum. The computational modeling of this interaction involved two distinct steps: (a) geometrical modeling of the instrumented horizontal mine-impulse pendulum and (b) a non-linear dynamics analysis of the momentum transfer from the detonation-products/soil ejecta to the pendulum.

Various computational domains used in the present study are shown in Fig. 2. The geometrical models for the various components of the pendulum were constructed using 50 mm × 50 mm square shell elements. An advantage was taken of the planar symmetry of the model. In other words, a vertical plane of symmetry was placed along the length of the pendulum, which enabled only a half of the pendulum to be modeled. In accordance with the instrumented horizontal mine-impulse pendulum used in Ref. [15], different sections of the pendulum were constructed using AISI 1006 steel and (rolled Homogenized Armor) RHA plate material. Welded joints of the different sections of the pendulum were simulated by joining the components in question.

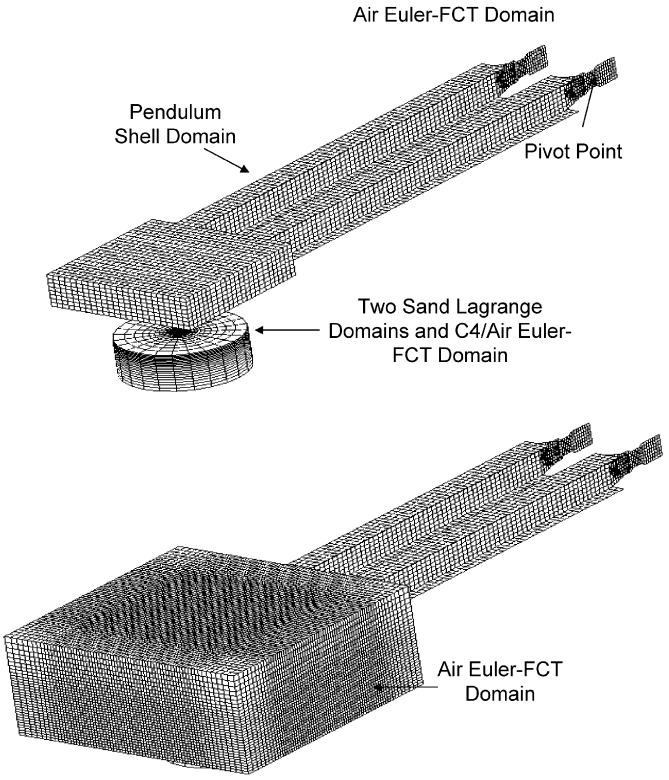

Fig. 2. Various computational domains used in the present non-linear dynamics analysis of the interactions of the detonation products, mine fragments and sand ejecta with the horizontal mine-impulse pendulum [15].

The head of the pendulum was placed in an Euler-FCT region consisting of 74,000 25 mm edge-length cubic cells. The Euler-FCT processor is a single material processor in which materials are combined to a single material using a flux corrected transport (FCT) approach and is generally used to handle computationally intensive multi-material blast phenomena. In the case of a surface laid mine, the mine was represented by a high-density high-energy cylindrical air region located within the Euler-FCT domain. In the case of a shallow-buried mine, two joined Lagrange domains were used to define a sand region containing a cylindrical cavity whose shape and size match those of the C4mine. A second Euler-FCT domain overlapping with the two sand domains is defined and the portion of this domain corresponding to the cylindrical sand cavity defined above is initially filled with high-density high-energy air.

The air/sand and air/pendulum interactions are accounted for using the appropriate Euler/Lagrange coupling option with AUTODYN [13]. Likewise, the sand/pendulum interactions were modeled through the use of the appropriate Lagrange/Lagrange coupling option.

A standard mesh-sensitivity analysis was carried out (the results not shown for brevity) in order to ensure that the results obtained are insensitive to the size of the cells used. Similar mesh-sensitivity analyses were carried out for the remaining studies presented in this paper.

At the beginning of the simulation, the pendulum is assumed to be at rest (with the gravitational force acting downwards), while the Lagrange and Euler-FCT domains are filled with stationary materials (sand and air, respectively). The internal energy and the density of the detonation products were obtained by setting them equal to their counterparts in the case of solid C4 explosive. In the initial simulations, the mine casing was considered explicitly. After it was determined that its contribution to the overall momentum transfer is negligible, subsequent simulations were carried out without explicitly representing the mine casing.

The motion of the pendulum was constrained to within a vertical plane and a fixed single-point constraint was applied to its pivot point. The "flow out" boundary conditions were applied to all the free faces (the faces which do not represent interfaces between the different domains) of the Euler-FCT domain except for the face associated with the vertical symmetry plane. To reduce the effect of reflection of the shock waves at the outer surfaces of the Lagrange domain, "transmit" boundary conditions were applied to all the free faces of this domain except for the face associated with the vertical symmetry plane. Also, to include the effect of gravity, a density and gravitational acceleration proportional body forces are distributed throughout the participating materials.

To speed up the calculations, all Euler-FCT and Lagrange domains were removed from the analysis after approximately 10 ms following detonation when the extent of interaction between the detonation-products/sand ejecta and the pendulum was negligibly small.

The effect of the degree of saturation in sand on the total impulse transferred to the pendulum in the case of sand containing various levels of moisture for four different DOBs of the C4mine obtained in Ref. [15] is displayed in Fig. 3(a) and (b). The total impulse associated with the horizontal instrumented mine-impulse pendulum is calculated using the formulation provided in [19] and is based on the maximum angular displacement experienced by the pendulum.

The 0 cm DOB corresponds to a "flush-buried" mine while the −5 cm DOB corresponds to a "ground-laid" mine. Also displayed in Fig. 3(a) and (b) are the computational results obtained in the present work using both the original sand compaction model and the present CU-ARL sand model. The results displayed in Fig. 3(a) and (b) can be summarized as follows:

(a) The model/experiment agreement is somewhat improved when the original porous-material model is replaced with the CU-ARL sand model for all landmine detonation cases analyzed.
(b) The lowest value of the impulse transferred to the horizontal instrumented mine-impulse pendulum is obtained in the case of a ground-laid mine (Fig. 3(a)) since this transfer takes place almost exclusively via the interaction of the gaseous detonation products with the pendulum. This is supported by the fact that the impulse transferred to the pendulum is essentially independent of the degree of saturation. The observed dependence of the total impulse on the degree of saturation (Fig. 3(a)) suggests that, even for the ground-laid mine case, measurable interactions between the detonation products and the underlying soil take place leading to the energy absorption by sand. Such energy absorption is lower in the case of saturated sand.
(c) For a flush-buried mine (0 cm DOB) (Fig. 3(a)) the detonation-induced impulse transfer is increased since, in addition to the detonation products, sand ejecta also interact with the pendulum.
(d) The largest impulse transfer occurs in the case of shallow-buried mines (5 and 10 cm DOB) (Fig. 3(b)) where the extent of sand ejection and interaction with the pendulum is the largest.
(e) Since the total impulse transferred to the pendulum is somewhat larger for the case of 5 cm DOB than that in the case of 10 cm DOB, it appears that there is an optimum DOB which maximizes the lethal effect of detonation of a shallow-buried mine. This can be rationalized by the fact that as the DOB is increased the effects of detonation become more confined within the soil (the "camouflet effect").
(f) The overall quantitative agreement between the CU-ARL model-based computational results and their experimental counterparts at different values of DOB

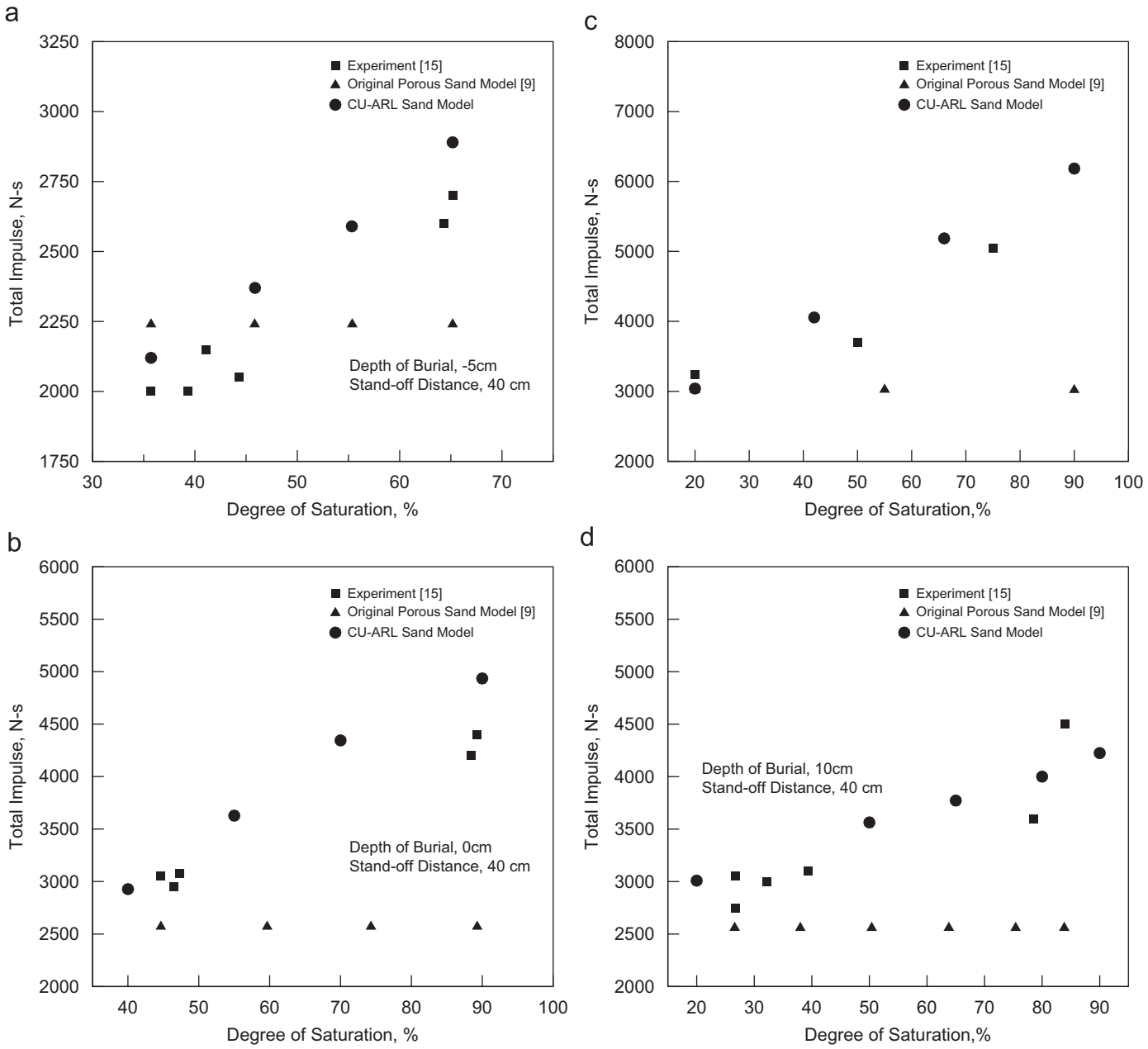

Fig. 3. The effect of degree of saturation on the total impulse transferred to the instrumented horizontal mine-impulse pendulum for the depths of burial of (a) −5 cm, (b) 0 cm, (c) 5 cm and (d) 10 cm.

is reasonable considering the fact that a noticeable disagreement between the computational and the experimental results is seen in the −5 cm DOB case (Fig. 3(a)) where the choice of the materials model for sand is essentially inconsequential since only the gaseous detonation products interact with the pendulum.

3.1.2. Saturated sand

To assess the ability of the CU-ARL sand model to account for the total momentum transferred to the target structure at high saturation levels of the sand, a non-linear dynamics-based computational analysis of the interaction of detonation products, mine fragments and sand ejecta with a vertical impulse measurement fixture used in Ref. [16], is carried out and the computed results are compared with their experimental counterparts. Since a detailed description of the experimental details related to the construction and utilization of the vertical impulse measurement fixture can be found in our recent work [11], they will not be presented here.

The basic formulation of the computational problem dealing with the interactions between the detonation products, shell fragments and soil ejecta (all resulting from the explosion of a shallow-buried landmine) and the VIMF [17,18] is presented next. The computational modeling of

this interaction involved two distinct steps: (a) geometrical modeling of the VIMF along with the adjoining mine, air and sand regions, and (b) the associated transient non-linear dynamics analysis of the impulse loading (momentum transfer) from the detonation products, shell fragments and soil ejecta to the VIMF structure (Fig. 4). The part (b) of this analysis was performed using a modified version of the technique developed by Fairlie and Bergeron [19]. This technique couples a multi-material Eulerian mesh to three Lagrangian meshes. The Eulerian mesh contained initially a TNT mine (and after mine explosion the resulting high-pressure, high-internal energy-density detonation products) and the (initially stationary, atmospheric-pressure) air. The mesh was constructed in terms of eight-node elements. One of the Lagrangian mesh was used to model the soil, the other to represent the VIMF witness plate while the third one was used to model the remainder of the VIMF structure. The soil and the VIMF structure were modeled using eight-node solid elements, while the witness plate was modeled using four-node shell elements.

An advantage was taken of the inherit symmetry of the model. In other words, two mutually orthogonal vertical planes of symmetry were placed along the axis of the VIMF as well as along the axis of the air, mine and sand regions which enabled only a quarter of the computational model to be analyzed. Representative quarter symmetric models for various computational domains used in the present study are shown in Fig. 5. It should be noted that the lower portion of the Eulerian domain contains the landmine while the rest of the lower portion of the Eulerian domain is occupied by the Lagrangian soil mesh. Likewise, the upper portion of the Eulerian domain, which extends above the soil, contains initially air and is partially occupied by the Lagrangian witness plate and VIMF meshes.

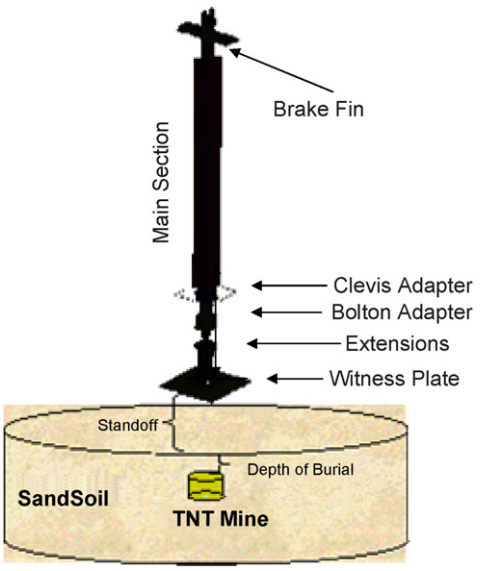

Fig. 4. A schematic of the vertical impulse measurement fixture (VIMF).

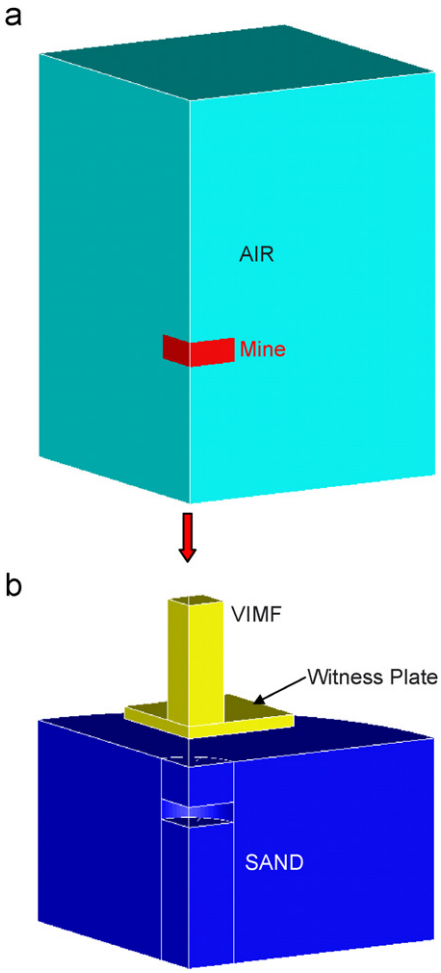

Fig. 5. Various computational domains used in the present non-linear dynamics analysis of the interactions of the detonation products, mine fragments and sand ejecta with the VIMF.

At the beginning of the simulation, all the Lagrange and Euler domains were activated and the landmine detonated. The (circular-disk shape) mine was detonated over its entire bottom face at the beginning of the simulation.

Next, a comparison is presented between the computational results for the VIMF obtained in the present work (found by integrating the momentum trace associated with the pendulum structure obtained from AUTODYN) and their experimental counterparts obtained by Taylor et al. [16]. The test conditions used in the work of Taylor et al. [16] are summarized in Table 1. It should be noted that two different witness plates were used with the respective length by width by thickness dimensions of $2.43\,m \times 2.82\,m \times 0.088\,m$ and $1.83\,m \times 3.65\,m \times 0.088\,m$.

A comparison between the experimental results and their computational counterparts is given in Table 2. To demonstrate the quantitative improvements brought about by the CU-ARL model for sand, the corresponding computational results obtained using the original compaction model are also shown in Table 2. An examination of the results shown in this table reveals that for each of the test conditions studied by Taylor et al. [16], the use of the

Table 1
VIMF set-up and test conditions [16]

Test no.	Charge mass (kg)	Charge diameter (m)	Charge height (m)	DoB[a] (m)	HoT[b] (m)	VIMF target total mass (kg)
1[c]	4.54	0.254	0.56	0.10	0.40	12,506
3[c]	4.54	0.254	0.56	0.30	0.40	12,506
4[c]	4.54	0.254	0.56	0.10	0.20	12,506
4a[d]	4.54	0.254	0.56	0.10	0.20	11,852
5[d]	2.27	0.152	0.76	0.80	0	11,852
6[d]	4.54	0.254	0.56	0.10	0.40	11,852
7[d]	2.27	0.152	0.76	0.81	0.16	11,535
8[d]	7.47	0.236	0.86	0.10	0.40	11,535

[a]DoB: depth of burial.
[b]HoT: height of the Target plate above the soil.
[c]Witness plate size: 2.43 m × 2.82 m × 0.088 m.
[d]Witness plate size: 1.83 m × 3.65 m × 0.088 m.

Table 2
Measured and computed impulse transferred to the VIMF witness plate

Test no.	Measured total impulse (N s)	Computed total impulse CU-ARL sand model (N s)	Computed total impulse compaction sand model (N s)
1	71,801	78,014	24,179
3	74,017	64,561	23,471
4	81,125	83,622	26,885
4a	69,644	57,174	22,368
5	77,612	72,448	25,251
6	59,286	64,452	19,042
7	36,938	37,689	12,017
8	94,390	86,042	29,705

CU-ARL model for sand yields an improved agreement with the experimental findings. In some cases, e.g. test numbers 4 and 7, the agreement between the model predictions and their experimental counterparts is exceptionally good. As discussed in our previous work [12], the main two reasons for the original compaction model for sand under-predicting the magnitude of the transferred impulse at high levels of the moisture content are: (a) too high compressibility of the sand which promotes explosion-energy dissipation through irreversible compaction of the sand and (b) a lack of consideration of the reduction of the sand's yield stress due to moisture-induced inter-particle lubrication effects which limits the extent of sand ejection.

3.2. Spatial and temporal evolution of sand-overburden bubble and pressure fields

To further assess the validity of the CU-ARL sand model to account for the spatial and temporal evolutions of the sand-overburden bubble and the pressure fields, following detonation of a ground-laid or shallow-buried mine at different saturation levels of the sand, the computational results are compared with their experimental counterparts obtained in Ref. [20]. In this section, a brief overview of the experimental set-up and the procedure used in Ref. [20] is first presented.

The experiments carried out in Ref. [20] can be briefly described as follows: A 1.27 cm wall thickness cylindrical barrel with the outer diameter of 81.6 cm and the overall height of 71 cm is filled with sand up to its top. A 100 g cylindrical-disk shape C4 high-energy explosive (6.4 cm in diameter and 2 cm in height) is buried into the sand along the centerline of the barrel with its faces parallel with the sand surface. The DOB (defined as the vertical distance between the top face of the explosive and the sand surface) is varied in a range between 0 and 8 cm. Thus, a 0 cm DOB case corresponds to a flush-buried explosive. A set of six pressure transducers is utilized to monitor the pressure in the air following the detonation of the explosive. The designations and the position coordinates of the six transducers are given in Table 3. The first number in the pressure transducer (PT) designation represents the distance in centimeters of the transducer from the origin of the coordinate system (defined below), while the second number represents the angular relation in degrees between the position vector of the pressure transducer and the axis of symmetry. The location of the six pressure transducers is also shown in Fig. 6. To be consistent with the definition of coordinate system for the 2D axi-symmetric problem used in AUTODYN [13], the y-coordinates are measured in the radial direction from the centerline of the barrel, while the x-coordinates are measured along the axis of symmetry, with $x = 0$

Table 3
Coordinates of the pressure transducers located in air

Transducer designation	Transducer coordinates (cm)	
	x	y
PT_30_0	−30.00	0
PT_30_22.5	−27.71	11.48
PT_30_45	−21.21	21.21
PT_70_0	−70.00	0
PT_70_30	−60.62	35.00
PT_110_0	−110.00	0

The origin of the coordinate system is located along the line of symmetry at the sand/air interface.

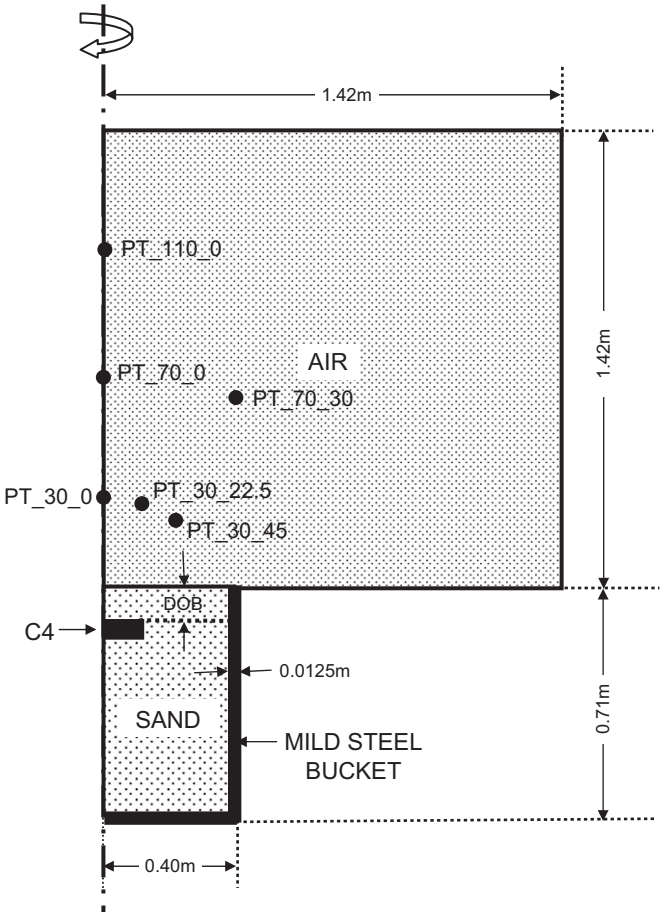

Fig. 6. A simple schematic of the experimental setup used in Ref. [20] to study the effect of explosion of a shallow-buried mine.

corresponding to the sand surface and $x<0$ denoting the air region above the ground.

The physical model displayed in Fig. 6 has been represented using the computational multi-material Euler model shown in Fig. 7. In Fig. 7, various portions of the computational domain are filled with one or more of the attendant materials (air, sand, C4 gaseous-detonation products and AISI 1006 mild steel). Due to the inherent axial symmetry of the set-up used in Ref. [20], the mine detonation is analyzed as a 2D axi-symmetric problem.

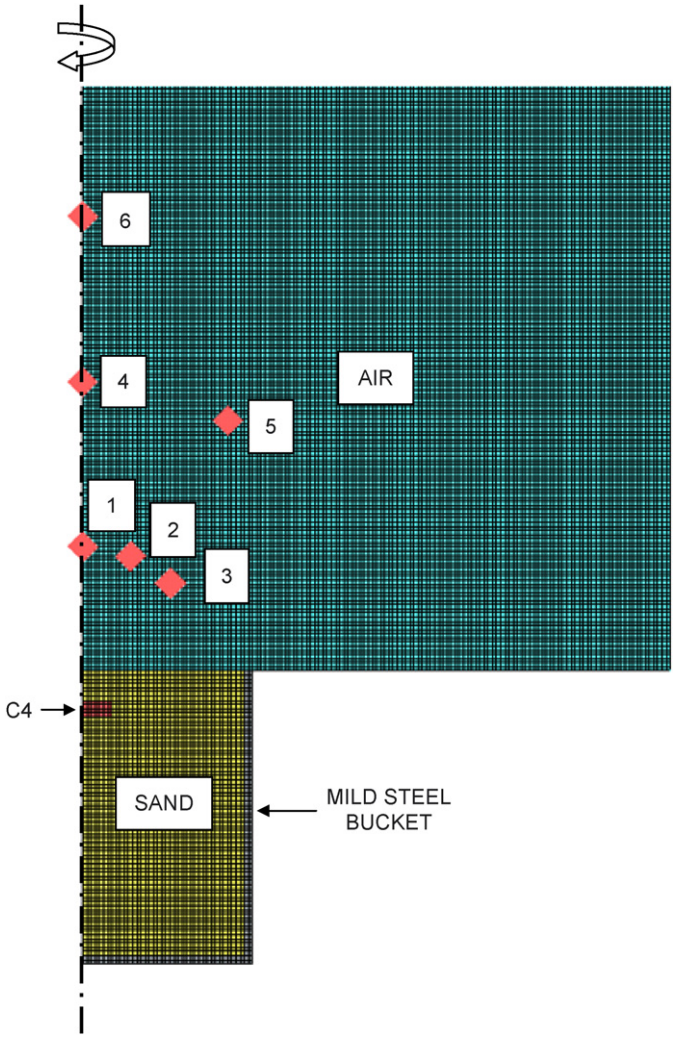

Fig. 7. Various computational domains used in the study of the effect of the explosion of a shallow-buried mine, Ref. [20].

The left boundary in Fig. 7 coincides with the axis of symmetry (x-axis). The horizontal direction (y-axis) corresponds to the radial direction.

The "flow-out" boundary conditions are applied to all the outer boundaries of the computational domain. To mimic the detonation initiation conditions used in Ref. [20], detonation is initiated at the central circular portion of the explosive of radius 3.2 cm, at the bottom face of the mine. To monitor the temporal evolution of pressure in air, six gage points are introduced whose locations coincide with those of the pressure transducers used in Ref. [20].

The ability of the CU-ARL model for sand to account for the main observations obtained during experimental investigation of landmine detonation in "dry" sand (average degree of saturation $\beta_0 = 0.15$) [20] is discussed first. A comparison of the computational and experimental results pertaining to the stand-off distance dependence of the peak overpressure and the time of blast-wave arrival (along the axis of symmetry), the angular dependence of the time of arrival and the temporal evolution of the

sand-overburden bubble height are shown respectively in Fig. 8(a)–(d). The results displayed in Fig. 8(a)–(d) can be summarized as follows:

(a) The model/experiment agreement is somewhat improved when the original porous-material model is replaced with the CU-ARL sand model for all landmine detonation cases analyzed.
(b) At a given value of the stand-off distance, the peak side-on (static) overpressure (the difference between the absolute pressure and the atmospheric pressure) decreases as the DOB increases (Fig. 8(a)). This is the result of the fact that as the thickness of the sand-overburden increases, a larger fraction of the potential energy contained within the high-pressure detonation products is absorbed by the compacting sand. Furthermore, at a given DOB, the peak overpressure decreases with an increase with the transducer distance from the air/sand interface as a result of various blast-wave attenuation and dispersion processes. The agreement between the CU-ARL model-based computational results and their experimental counterparts is reasonable in the case of 3 and 8 cm DOBs. However, the agreement is only fair in the case of 0 cm DOB. This may not be solely the result of the potential deficiencies of the present material model for

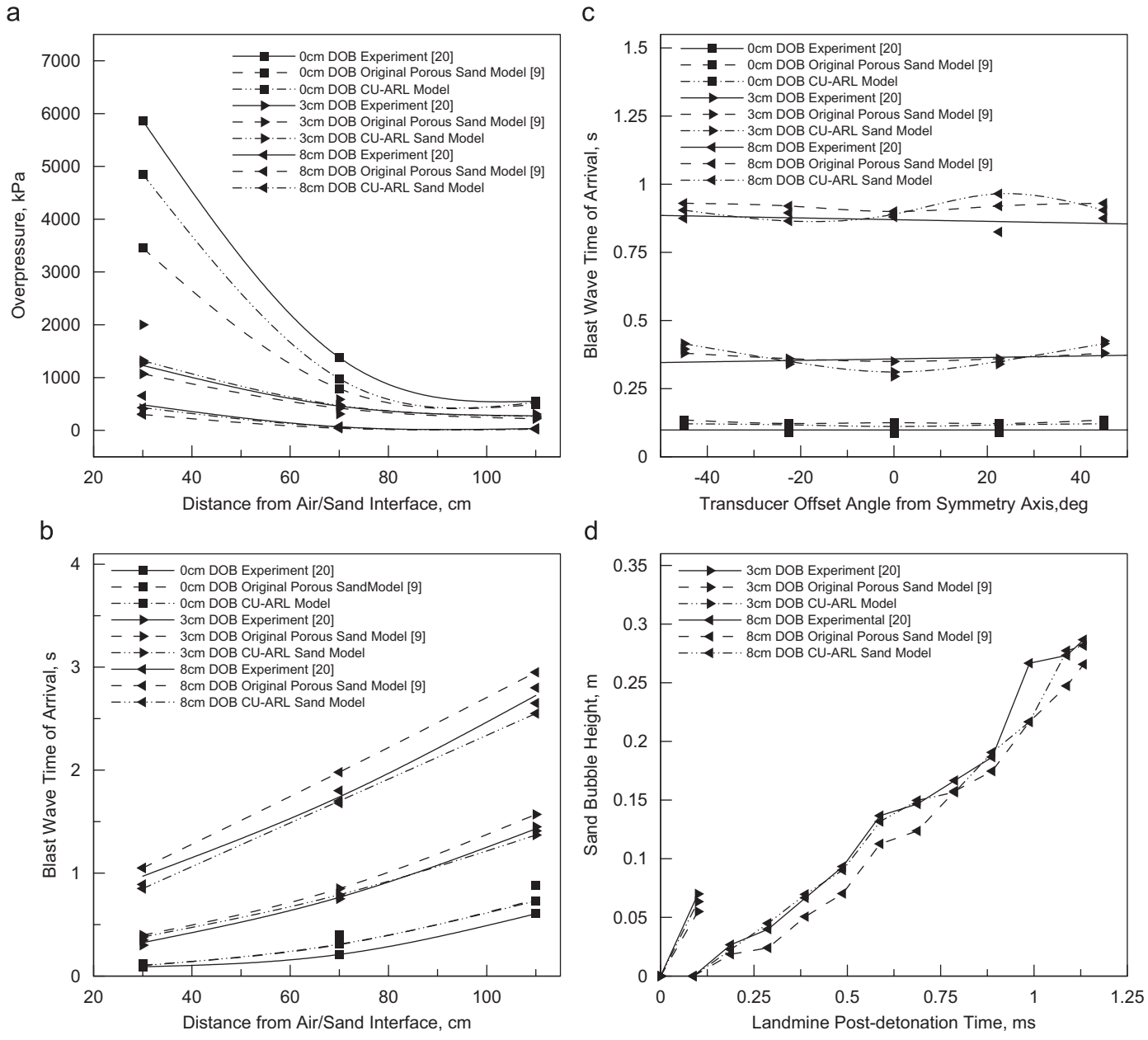

Fig. 8. A comparison of the experimental [20] and computed (present work) results pertaining to various phenomena associated with landmine detonation in dry sand: (a) side-on overpressure vs. transducer distance from air/sand interface, (b) blast wave arrival time vs. transducer distance from air/sand interface, (c) blast wave arrival time vs. transducer offset angle from the symmetry axis and (d) sand bubble height vs. landmine post-detonation time.

sand since the role of sand is least critical in the case of flush-buried mines. It should be noted that AUTODYN has been benchmarked against a standard aluminum-projectile, aluminum-target impact cratering experiment both for short-time and late-time simulations and the results obtained fully validate the computational procedure used in this code [21]. However, no literature regarding benchmarking of AUTODYN for blast events has been reported in open literature.

(c) At a given value of the stand-off distance, the time of arrival of the blast waves increases with an increase in DOB (Fig. 8(b)). This is the result of the fact that as the DOB increases, the distance between a given pressure transducer and the explosive also increases. For the same reason, at a fixed value of DOB, the time of arrival increases with an increase in the transducer distance from the air/sand interface. At the DOBs of 3 and 8 cm, the agreement between the CU-ARL model-based computational and experimental results is reasonable. On the other hand, at 0 cm DOB the agreement is less satisfactory. This may be, at least partly, caused by the fact that due to the large magnitude of blast pressures in the case of flush-buried

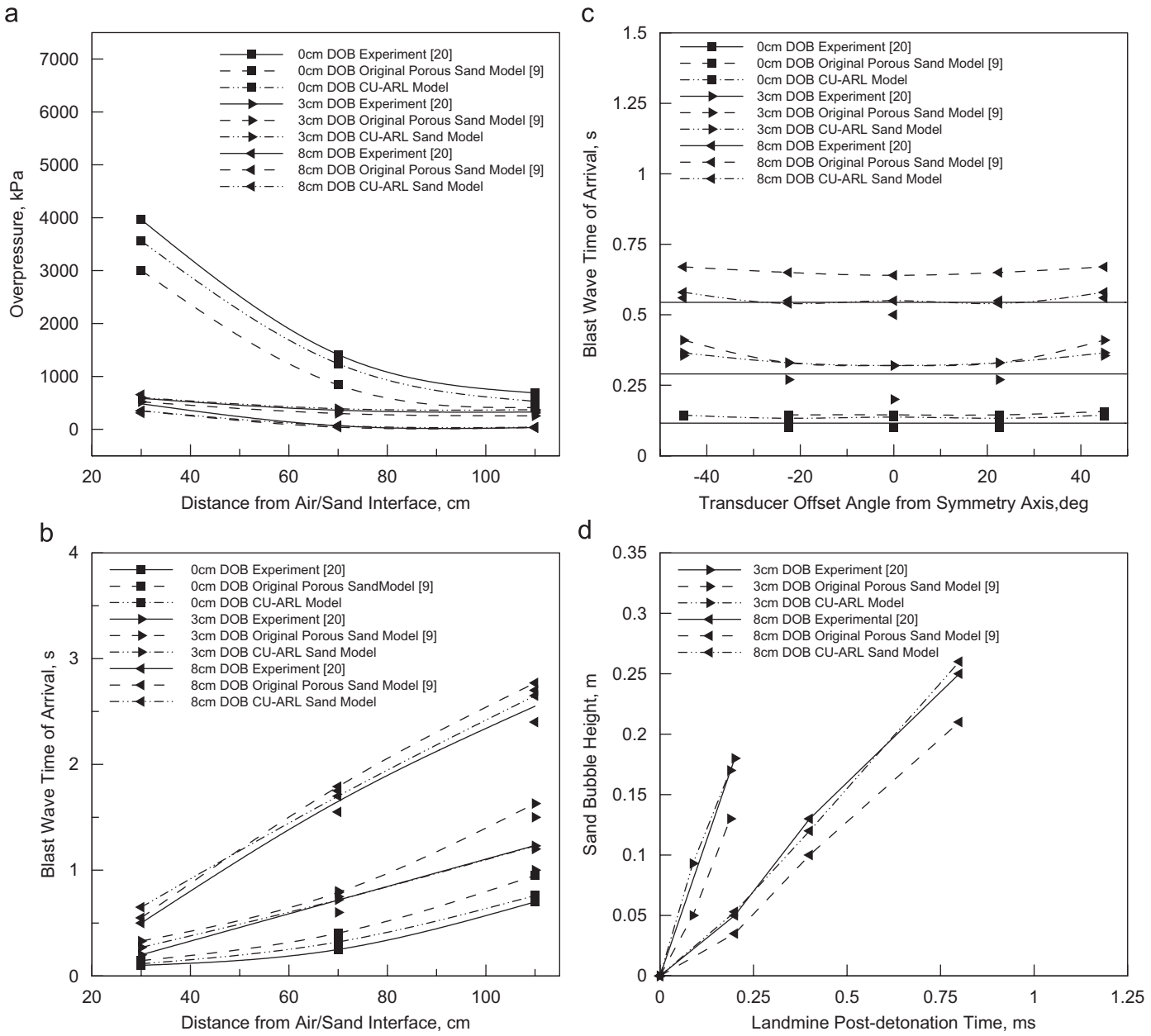

Fig. 9. A comparison of the experimental [20] and computed (present work) results pertaining to various phenomena associated with landmine detonation in fully saturated sand: (a) side-on overpressure vs. transducer distance from air/sand interface, (b) blast wave arrival time vs. transducer distance from air/sand interface, (c) blast wave arrival time vs. transducer offset angle from the symmetry axis and (d) sand bubble height vs. landmine post-detonation time.

mine, transducer signals contained a lot of noise making precise estimation of the arrival time (as well as peak pressures) quite difficult.

(d) At a given value of DOB, the time of arrival of the blast waves is quite insensitive to the offset angle of the transducer from the symmetry axis (Fig. 8(c)). This could be explained by the fact that while the offset angle is varied, the offset distance (the distance between the top center point of the mine and the transducer) was kept constant. At each of the three values of the DOB, the agreement between the CU-ARL model-based computational and experimental results is reasonable.

(e) The agreement between the CU-ARL model-based computational and the experimental results pertaining to the temporal evolution of sand bubble height is very good in the case of 8 cm DOB (Fig. 8(d)). In the case of 3 cm DOB, the agreement is also good but caution should be exercised from drawing conclusions due to a limited number of experimental data points. Further, it should be noted that due to the absence of sand-overburden in the case of 0 cm DOB, no sand bubble is formed during landmine detonation.

The ability of the present material model for sand to account for the main observations obtained during experimental investigation of landmine detonation in fully saturated sand (average degree of saturation $\beta_0 \sim 1.0$) [20] is discussed next. A comparison of the computational and experimental results pertaining to the stand-off distance dependencies of the peak overpressure and the time of blast-wave arrival (along the axis of symmetry), the angular dependence of the time of arrival and the temporal evolution of the sand-overburden bubble height are shown, respectively, in Fig. 9(a)–(d). The agreement between the computational results and their experimental counterparts displayed in Fig. 9(a)–(d) can be summarized as follows:

(a) The model/experiment agreement is somewhat improved when the original porous-material model is replaced with the CU-ARL sand model for all landmine detonation cases analyzed.

(b) In the case of peak overpressure vs. transducer distance from air/sand interface results (Fig. 9(a)) the agreement between the CU-ARL model-based computational and experimental results is reasonable in the case of 3 and 8 cm DOBs. In the case of 0 cm DOB (the case associated with the largest uncertainty in the experimental results), on the other hand, the agreement is only fair. It should be also pointed out that in the case of 0 cm DOB and 30 cm stand-off distance, the observed good agreement is most likely fortuitous. This conjecture is based on two observations: (i) the transducer in question showed visible signs of mechanical wear and damage, at the time when mine-detonation experiments in saturated soil were carried out [20] and (ii) the experimental values for the pressure ($\sim$4000 kPa), in the case of saturated soil are inexplicably substantially lower than its counterpart in dry soil ($\sim$6000 kPa).

(c) In the case of the time of arrival vs. stand-off distance results, the agreement between the CU-ARL model-based computational and experimental results is reasonable for all three values of DOB (Fig. 9(b)).

(d) Both the experimental and the computational results show that the time of arrival of the blast waves increases with an increase in the offset angle of the transducer from the symmetry axis (Fig. 9(c)). However, the quantitative agreement between the two sets of results is only fair at each of the three DOBs.

(e) In the case of the height of sand bubble vs. landmine post-detonation time results (Fig. 9(d)), the agreement between the CU-ARL model-based computational and the experimental results is only fair.

4. Discussion

The results presented in Sections 3.1 and 3.2 suggest that the CU-ARL sand model when used in conjunction with the appropriate transient non-linear dynamics simulations can reasonably well account for the magnitude, spatial distribution and temporal evolution of the dynamic loads accompanying detonation of shallow-buried mines in soil with various levels of clay and water contents. In the case of detonation of flush-buried mines, the effect of the material model for sand is expected to be less pronounced and, hence, less critical. Consequently, the observed discrepancies between the experimental and the computational results in the case of 0 cm DOB cannot be readily interpreted as the shortcomings of the sand material model. This conclusion is further supported by the fact that the corresponding experimental results were associated with substantial uncertainty (typically the standard deviation was 25–30% of the mean value). Also, there are additional phenomena, which were not accounted for in the transient non-linear dynamics analysis of the mine detonation. For instance, dynamic pressure, in addition to the static pressure, can contribute to the transducer signal; evaporated water can significantly alter the properties of air, etc. It is interesting to note that the two aforementioned phenomena are expected to be most prevalent in the case of 0 cm DOB and the saturated soil, the case associated with the largest mismatch between the experimental and the computational results.

The extent of agreement between the CU-ARL model-based computational results and experimental results can be considered reasonably good considering the fact that the soils used in the three sets of experiments had varying amounts of clay and other inorganic and organic matter, as well as different average particle size and particle size distributions.

Finally, it is interesting that the CU-ARL sand model can account for the experimentally well-established

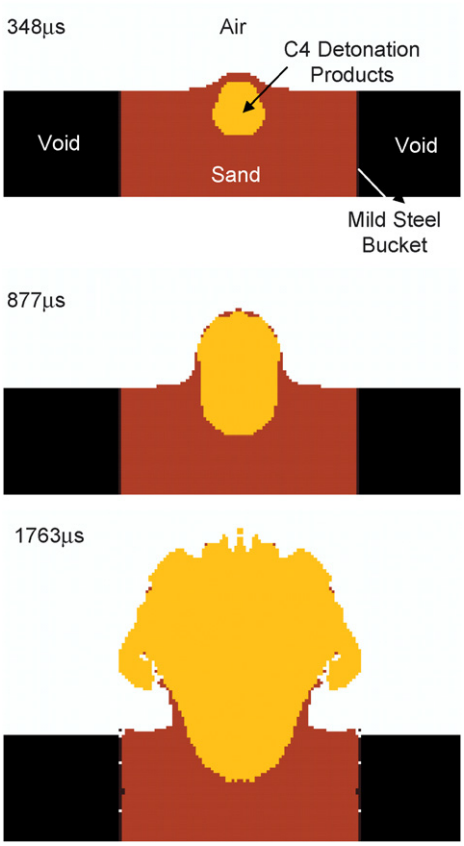

Fig. 10. Typical temporal evolution of material deformation during landmine detonation in the case of dry sand.

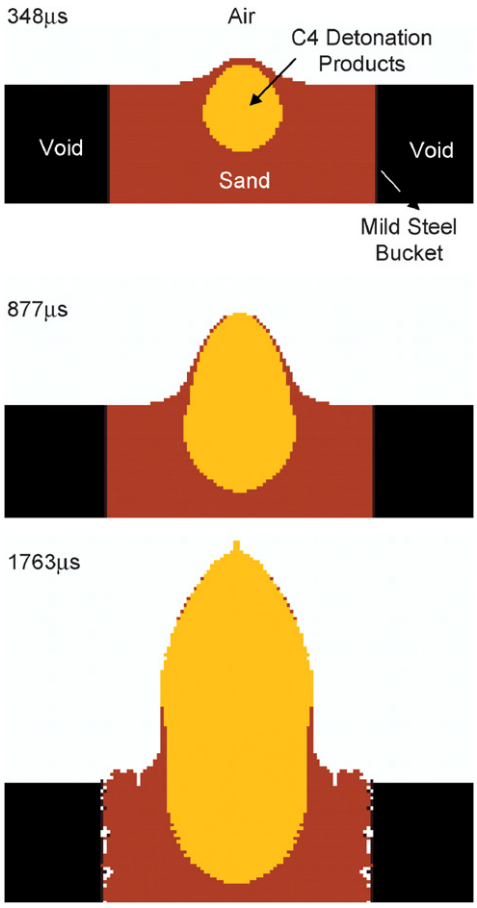

Fig. 11. Typical temporal evolution of material deformation during landmine detonation in the case of fully saturated sand.

differences in blast-loads distribution and the material evolution following landmine detonation in the dry sand (Fig. 10(a)–(c)) and saturated sand (Fig. 11(a)–(c)). It is evident that in the case of dry sand (Fig. 10(a)–(c)), the sand-overburden fractures earlier allowing venting of gaseous detonation products. In sharp contrast, Fig. 11(a)–(c) shows that in the case of saturated sand, sand-overburden resists fracture and produces a tunneling effect (i.e. concentration of blast loads in the upward direction). This prediction combined with the observed differences in the crater size (Fig. 10(c) vs. Fig. 11(c)), and the extent of sand compaction, is in complete agreement with general experimental observations that saturated-sand landmine detonation produces higher and more localized dynamic loads.

5. Summary and conclusions

Based on the results obtained in the present work, the following main summary remarks and conclusions can be drawn:

1. Experimental results obtained by researchers at the Cavendish laboratory [1,2] were used to parameterize the equation of state for sand at different levels of saturation and the resulting material model for sand has shown significant differences relative to the standard compaction model for sand developed by Laine and Sandvik [9].
2. A number of landmine detonation computational analyses have been conducted using both the original sand compaction model [12] and the CU-ARL model [3] and the computational results confirm that the degree of saturation of sand indeed plays an important role in its mechanical response during impact/blast loading.
3. Overall, the computational experiment agreement is improved. When the original sand compaction model is replaced by the CU-ARL model and the extent of agreement between the CU-ARL model-based computational results and their experimental counterparts is reasonable.
4. Several additional causes for observed computational/experimental discrepancies beyond those that could be designated as the sand-model shortcomings have been identified (e.g. effect of dynamic pressure on the readings of the pressure transducer, the effect of moisture content on the constitutive response of sir above the explosion site, etc.).

Acknowledgments

The material presented in this paper is based on work supported by the US Army/Clemson University Cooperative

Agreements W911NF-04-2-0024 and W911NF-06-2-0042 and by the US Army Grant Number DAAD19-01-1-0661. The authors are indebted to Dr. Fred Stanton for the support and a continuing interest in the present work.

References

[1] Bragov AM, Lomunov AK, Sergeichev IV, Tsembelis K, Proud WG. The determination of physicomechanical properties of soft soils from medium to high strain rates, November 2005, in preparation.
[2] Chapman DJ, Tsembelis K, Proud WG. The behavior of water saturated sand under shock-loading. In: Proceedings of the 2006 SEM annual conference and exposition on experimental and applied mechanics, vol. 2, 2006. p. 834–40.
[3] Grujicic M, Pandurangan B, Cheeseman B. The effect of degree of saturation of sand on detonation phenomena associated with shallow-buried and ground-laid mines. J Shock Vib 2006;13:41–61.
[4] Wang Z, Hao H, Lu Y. A three-phase soil model for simulating stress wave propagation due to blast loading. Int J Numer Anal Meth Geomech 2004;28:33–56.
[5] Wang Z, Lu Y. Numerical analysis on dynamic deformation mechanisms of soils under blast loading. Soil Dyn Earthquake Eng 2003;23:705–14.
[6] Loret B, Khalili N. A three-phase model for unsaturated soils. Int J Numer Anal Methods in Geomech 2000;24:893–927.
[7] Henrych J. The dynamics of explosion and its use. New York, USA: Elsevier Publications; 1979 [chapter 5].
[8] Drucker DC, Prager W. Soil mechanics and plastic analysis or limit design. Quart Appl Math 1952;10:157–65.
[9] Laine P, Sandvik A. Derivation of mechanical properties for sand. In: Proceedings of the fourth Asia–Pacific conference on shock and impact loads on structures. Singapore: CI-Premier PTE LTD, November 2001. p. 361–8.
[10] Grujicic M, Pandurangan B, Cheeseman BA. A computational analysis of detonation of buried mines. Multidiscipline Modeling in Materials and Structures 2006;2:363–87.
[11] Grujicic M, Pandurangan B, Huang Y, Cheeseman BA, Roy WN, Skaggs RR. Impulse loading resulting from shallow buried explosives in water-saturated sand. Journal of Materials: Design and Applications 2006;220:1–15.
[12] Grujicic M, Pandurangan B, Summers JD, Cheeseman BA, Roy WN. Application of the modified compaction material model to soil with various degrees of water saturation. Shock and Vibration 2007;14:1–15.
[13] AUTODYN-2D and 3D. Version 6.1, user documentation. Century Dynamics Inc.; 2006.
[14] Stein S, Kim T. Effect of moisture on attraction force on beach sand. Mar Geosour Geotechnol 2004;22:33–47.
[15] Bergeron D, Tremblay JE. Canadian research to characterize mine blast output. In: Proceedings of 16th international MABS symposium, Oxford, UK, September 2000.
[16] Taylor LC, Skaggs RR, Gault W. Vertical impulse measurements of mines buried in saturated sand. Fragblast 2005;9(1):19–28.
[17] Gniazdowski N. The vertical impulse measurement facility maintenance and inspection manual. ARL technical report, 2004, submitted for publication.
[18] Skaggs RR, Watson J, Adkins T, Gault W, Canami A, Gupta AD. Blast loading measurements by the Vertical Impulse Measurement Fixture (VIMF). ARL technical report, submitted for publication.
[19] Fairlie G, Bergeron D. Numerical simulation of mine blast loading on structures. In: Proceedings of the 17th military aspects of blast symposium, Nevada, June 2002.
[20] Foedinger J. Methodology for improved characterization of landmine explosions. SBIR Phase-II Plus Program, technical interchange meeting, material science corporation, June 2005.
[21] Pierazzo E, Artemieva N, et al. The impact hydrocode benchmark and validation project: initial results. In: Proceedings of the 37th lunar and planetary science conference, League City, Texas, 2007.